AIAA JOURNAL
Vol. 45, No. 6, June 2007

Novel Boundary Integral Formulation for Blade–Vortex Interaction Aerodynamics of Helicopter Rotors

Massimo Gennaretti* and Giovanni Bernardini†
University Roma Tre, 00146 Rome, Italy

DOI: 10.2514/1.18383

A direct panel method based on a novel boundary integral formulation for the velocity potential is presented and applied to helicopter rotors experiencing blade–vortex interaction. It avoids the numerical instabilities arising in the standard direct panel method in case of blade/wake impingement. This aerodynamic formulation yields a unified approach for the calculation of free-wake evolution and the blade-pressure field; it is fully 3-D, includes body-thickness effects, and can be applied to blades with arbitrary shape and motion. Blade-pressure predictions and the corresponding acoustic fields correlate well with wind-tunnel test data for helicopter rotors in descent flight, in which severe blade–vortex interaction occurs.

Nomenclature

$\mathcal{C}$	=	panel contour
G	=	Green function
$\boldsymbol{n}$	=	unit outward normal vector on a surface
p	=	pressure
$\mathcal{S}$	=	surface
t	=	time
$\boldsymbol{v}$	=	velocity field
$\boldsymbol{x}$	=	observer position
$\boldsymbol{y}$	=	source position
ρ	=	air density
τ	=	time delay
φ	=	velocity potential
χ	=	body normal velocity component

Subscripts

B	=	body
I	=	incident field
S	=	scattered field
W	=	wake

Superscripts

F	=	far wake
N	=	near wake
TE	=	trailing edge

I. Introduction

IN PARTICULAR flight conditions, helicopter main rotor blades experience a phenomenon known as blade–vortex interaction (BVI), which consists of the passage of a rotor blade through the vortices released by the other blades of the rotor. Typical conditions at which this phenomenon occurs are descent flight and maneuvers at moderate advance ratio. The aerodynamic effects produced by BVI are impulsive changes in blade surface pressure distribution and are of particular importance in the blade regions in which the interaction occurs with the high-strength trailing-tip vortices [1]. In the last 20 years, many rotorcraft researchers focused their activity on the prediction of this phenomenon because these impulsive loads are one of the main sources of external noise and fuselage vibration; thus, they have a great impact on both the cabin acoustic comfort and on the environmental and public acceptance of helicopters. Hence, the availability of a reliable tool for the prediction of BVI aerodynamics is essential for new-generation helicopter design, in which reduction of both maintenance costs and noise level is of great interest.

Because the physics of the BVI are governed by the structure of the wake and by its distance from the rotor blade (miss distance), an aerodynamic formulation capable of capturing BVI has to take into account the real shape of the blades, has to analyze three-dimensional unsteady flows, and has to accurately predict the wake-shape evolution. Typically, prediction tools developed to examine rotorcraft in BVI conditions are based on the use of different codes for the free-wake analysis and for the computation of the pressure distribution on the blade (the latter is frequently based on 2-D airfoil aerodynamics). For instance, there is the study aimed at aeroelastic applications presented in [2], in which a multiple-trailer vortex model is used in the free-wake analysis to determine the induced flow correction to be applied to an aerodynamic load model based on thin airfoil theories. A similar approach is considered in [3] for aeroacoustic purposes, in which a vortex-lattice free-wake procedure is combined with a blade-element theory for section-load prediction, along with a system of low- and high-resolution grids to ensure a detailed analysis of BVI. The combined use of a dual-vortex free-wake code with a 2-D aerodynamics code is applied in [4] for the aeroelastic and aeroacoustic analysis of rotors for vibration and noise reduction purposes. In [5], the aerodynamic analysis of rotors in BVI conditions consists of a three-step procedure. The results of an initial vortex-lattice free-wake analysis are coupled with a roll-up model that identifies the higher-intensity vortex structure to be considered as the interacting vortices in a pressure predictor code based on a Euler 2-D solver. In the works mentioned earlier, the aerodynamic analysis follows a previous aeroelastic calculation that predicts the blade deformation. A fully 3-D aerodynamic formulation is applied in [6] to calculate the blade-pressure distribution for rotors in BVI conditions. It is an unsteady, indirect panel method that considers a vortex-lattice-deforming wake combined with a source/sink distribution of unknown strength over the blade surface (to simulate the displacement effect of blade finite thickness) and a doublet distribution of unknown strength over the camber surface inside the blade (to include section circulation).

The objective of this paper is to introduce a boundary integral formulation for the aerodynamic analysis of unsteady, potential flows that is suited for rotorcraft configurations in which blade/wake impingement occurs, and to validate it by correlation with

Presented as Paper 2924 at the 11st AIAA/CEAS Aeroacoustics Conference, Monterey, CA, 23–25 May 2005; received 24 June 2005; revision received 12 February 2007; accepted for publication 19 February 2007.

*Associate Professor, Mechanical and Industrial Engineering Department; m.gennaretti@uniroma3.it.
†Research Engineer.

experimental data. This formulation is developed by starting from the standard boundary integral approach for potential flows introduced in [7] and is related to that presented in [8]. The process of discretization of blade and wake surfaces yields a direct panel method for the numerical solution of the unknown potential field. The time evolution of the potential is achieved through a time-marching integration scheme during which the surface of the wake is continuously moved so as to be tangent to the corresponding velocity field (free-wake procedure). Akin to the indirect panel method of [6], the methodology presented here yields a unified approach for the evaluation of both wake distortion and the corresponding pressure field on the blade surfaces; it is fully three-dimensional, includes body thickness effects, can be extended to compressible flows [9,10], and then applied for unified aerodynamic/aeroacoustic analysis [11]. The novelty of this work lies in the following three points:

1) The way in which a wake simulated as a vortex lattice is included in a direct panel method for potential flows (which is considerably different from that in [8]).

2) The new methodology that is used for the evaluation of the pressure through a reformulation of the Bernoulli theorem.

3) A direct panel method is applied to configurations in which BVI occurs, through an implementation that facilitates the solution of an otherwise intractable problem (at least whenever the zero-thickness wake assumption cannot be applied).

For the sake of completeness, the standard boundary integral formulation is briefly described in the next section, before introducing the boundary integral formulation that is suited for rotors in BVI conditions. Numerical results from the present formulation are then correlated with experimental data concerning helicopter rotors in descent flight with severe BVI occurrence. The comparison is given both in terms of blade-pressure distributions and in terms of the acoustic fields generated by the rotors.

This work was developed within the context of the European Union Integrated Project FRIENDCOPTER, which promotes environmental friendliness and public acceptance of helicopters through reduction of noise emission, gas exhaust, and cabin noise levels. In particular, such a work is included in a broader activity that deals with the definition of procedures for noise abatement.

II. Standard Boundary Integral Formulation

For unsteady, incompressible, quasi-potential flows (i.e., potential everywhere except on the wake surface) around lifting bodies in arbitrary motion with respect to the undisturbed air, the velocity potential field may be expressed by the following boundary integral representation [7]:

$$\varphi(\boldsymbol{x},t)=\int_{\mathcal{S}_B}\left(G\frac{\partial\varphi}{\partial n}-\varphi\frac{\partial G}{\partial n}\right)\mathrm{d}\mathcal{S}(\boldsymbol{y})-\int_{\mathcal{S}_W}\Delta\varphi\frac{\partial G}{\partial n}\mathrm{d}\mathcal{S}(\boldsymbol{y}) \tag{1}$$

where $\mathcal{S}_B$ and $\mathcal{S}_W$ are body and wake surfaces, respectively. The impermeability boundary condition on $\mathcal{S}_B$ yields $\partial\varphi/\partial n=\boldsymbol{v}_B\cdot\boldsymbol{n}$, where $\boldsymbol{v}_B$ denotes the velocity of body points and $\boldsymbol{n}$ is on $\mathcal{S}_B$, whereas $G=-1/4\pi||\boldsymbol{y}-\boldsymbol{x}||$ is the free-space fundamental solution of the three-dimensional Laplace equation. In addition, $\Delta\varphi$ is the potential jump across the wake surface that is given by the Kutta–Joukowski condition [12], followed by convection of the trailing-edge potential discontinuity, that is,

$$\Delta\varphi(\boldsymbol{x}_W,t)=\Delta\varphi(\boldsymbol{x}_W^{\mathrm{TE}},t-\tau) \tag{2}$$

with τ denoting the time taken by a wake material point to move from the trailing-edge position $\boldsymbol{x}_W^{\mathrm{TE}}$ to its current position $\boldsymbol{x}_W$ (see [7] for details).

Equation (1) may be solved numerically by boundary elements (i.e., by discretizing $\mathcal{S}_B$ and $\mathcal{S}_W$ into quadrilateral panels), assuming φ, $\partial\varphi/\partial n$, and $\Delta\varphi$ to be piecewise constant, and imposing that the equation be satisfied at the center of each body element (collocation method). Specifically, dividing the blade surface into M panels $\mathcal{S}_{B_i}$, the wake surface into N panels $\mathcal{S}_{W_j}$, and for $\chi=\boldsymbol{v}_B\cdot\boldsymbol{n}$, Eq. (1) yields

$$\varphi_k(t)=\sum_{i=1}^{M}B_{ki}\chi_i(t)+\sum_{i=1}^{M}C_{ki}\varphi_i(t)+\sum_{j=1}^{N}F_{kj}\Delta\varphi_j(t) \tag{3}$$

where $\varphi_i(t)=\varphi(\boldsymbol{x}_i,t)$, $\chi_i(t)=\chi(\boldsymbol{x}_i,t)$, and $\Delta\varphi_j(t)=\Delta\varphi(\boldsymbol{x}_{W_j},t)$, and the source/sink and doublet coefficients are given by

$$B_{ki}=\frac{-1}{4\pi}\int_{\mathcal{S}_{B_i}}\left(\frac{1}{|\boldsymbol{y}-\boldsymbol{x}_k|}\right)\mathrm{d}\mathcal{S},\qquad C_{ki}=\frac{1}{4\pi}\int_{\mathcal{S}_{B_i}}\frac{\partial}{\partial n}\left(\frac{1}{|\boldsymbol{y}-\boldsymbol{x}_k|}\right)\mathrm{d}\mathcal{S}$$
$$F_{kj}=\frac{1}{4\pi}\int_{\mathcal{S}_{W_j}}\frac{\partial}{\partial n}\left(\frac{1}{|\boldsymbol{y}-\boldsymbol{x}_k|}\right)\mathrm{d}\mathcal{S} \tag{4}$$

For the analysis of configurations with BVI, Eq. (1) must necessarily be solved by determining the shape of the wake as a part of the solution (free-wake procedure). This is achieved by a time-marching integration scheme in which the vertices of the wake panels are moved according to the velocity field computed from the potential solution; thus, the wake coefficients F_{kj} are recomputed at each time step [8].

III. Novel Boundary Integral Formulation

The effectiveness of potential theory derives from the fact that vortical regions in many high-Reynolds-number flows of aeronautical interest are very thin (though not zero) and can be approximated by zero-thickness vortex structures. However, the numerical application of the potential theory, with its singular representation of vortical regions, would not yield the proper solution in the case of close wake-body interactions. Indeed, the numerical formulation based on Eq. (1) shows instabilities when the wake panels come too close to or impinge the body (i.e., just in BVI conditions). These instabilities are of numerical nature and are induced by the inaccuracy in evaluating the influence wake doublet coefficients F_{kj} when the wake panels approach body surface points.

Here, to overcome this problem, a novel potential-flow formulation is proposed. It is inspired by the observation that the instabilities arising in the numerical formulation when wake panels are too close to or impinge the body would be eliminated by replacing the wake influence coefficients F_{kj}, given in terms of doublet layers [see Eq. (4)], with equivalent finite core vortices. Indeed, the velocity field induced by a doublet distribution of uniform intensity γ over an arbitrary surface $\mathcal{S}$ equals that induced by a (closed) vortex filament located on the boundary of the surface $\partial\mathcal{S}$, also of intensity γ (see, for instance, [13–15], in which the more general equivalence between nonuniform doublet layers and vortex layers is proven). Then, if the vortex is assumed to have a finite core in which the induced velocity remains bounded, it yields a regular influence, even at body or wake points that approach it. Thus, the formulation introduced here is obtained by starting from the standard boundary integral formulation and then modeling the wake portion experiencing BVI as a finite thickness vortex lattice, rather than as a zero-thickness doublet surface [as in Eqs. (1) and (3)]. The theoretical development is explained in the following.

From the discretized version of the boundary integral representation, Eq. (3), combined with Eq. (2), it is possible to note that at a given time, the doublet distribution on the panels of the wake portion that is not in contact with the trailing edge (far wake $\mathcal{S}_W^F$, see Fig. 1) is known from the previous time steps and is not influenced by the current (unknown) potential over the body. Furthermore, the doublet distribution on the panels of the wake portion in contact with the trailing edge (near wake $\mathcal{S}_W^N$, see Fig. 1) is related to the jump of the current potential at the trailing edge of the blade [$\tau_j=0$ in Eq. (3) combined with Eq. (2)], but no BVI occurs in that wake region. At a given time, because the potential field induced by the far wake is unaffected by the current potential over the body and the near wake, it can be seen as an incident field that is scattered by the presence of the body and the near wake. This is the key point that allows redefining the far-wake contribution in the potential integral formulation in such a way that a regular solution is obtained

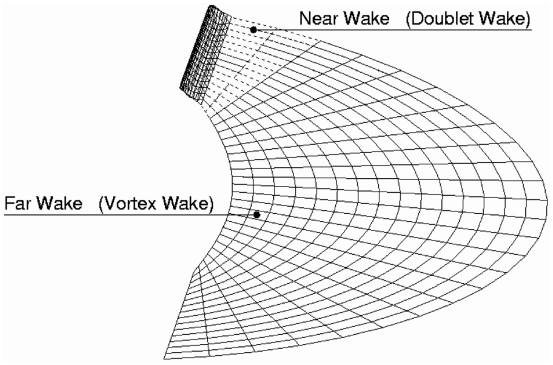

Fig. 1 Far-wake and near-wake decomposition.

during BVI occurrence. At each time, the potential field is decomposed into an incident field φ_I generated by doublets over $\mathcal{S}_W^F$ and a scattered field φ_S generated by sources and doublets over $\mathcal{S}_B$ and doublets over $\mathcal{S}_W^N$. This implies that for $\mathcal{S}_W = \mathcal{S}_W^N \cup \mathcal{S}_W^F$ and $\varphi = \varphi_I + \varphi_S$ with

$$\varphi_I(\boldsymbol{x}, t) = -\int_{\mathcal{S}_W^F} \Delta\varphi \frac{\partial G}{\partial n} \mathrm{d}\mathcal{S}(\boldsymbol{y}) \tag{5}$$

Eq. (1) yields

$$\varphi_S(\boldsymbol{x}, t) = \int_{\mathcal{S}_B} \left(G \frac{\partial \varphi}{\partial n} - \varphi \frac{\partial G}{\partial n} \right) \mathrm{d}\mathcal{S}(\boldsymbol{y}) - \int_{\mathcal{S}_W^N} \Delta\varphi \frac{\partial G}{\partial n} \mathrm{d}\mathcal{S}(\boldsymbol{y}) \tag{6}$$

where the dependence of the scattered potential on the incident one appears implicitly in the distribution of total potential over the body and near wake. To make this dependence explicit, let us consider a closed surface $\mathcal{S}_I$ surrounding the far wake. In the fluid region outside $\mathcal{S}_I$, the incident potential is governed by the Laplace equation $\nabla^2 \varphi_I = 0$. Thus, the application of the boundary integral approach in the exterior domain $\mathcal{V}_{\mathrm{EXT}}$ bounded by $\mathcal{S}_B \cup \mathcal{S}_I$ yields the following integral representation of the incident potential field for $\mathbf{x} \in \mathcal{V}_{\mathrm{EXT}}$:

$$\varphi_I(\boldsymbol{x}, t) = \int_{\mathcal{S}_B} \left(G \frac{\partial \varphi_I}{\partial n} - \varphi_I \frac{\partial G}{\partial n} \right) \mathrm{d}\mathcal{S}(\boldsymbol{y}) + \int_{\mathcal{S}_I} \left(G \frac{\partial \varphi_I}{\partial n} - \varphi_I \frac{\partial G}{\partial n} \right) \mathrm{d}\mathcal{S}(\boldsymbol{y}) \tag{7}$$

Near-wake contributions do not appear in Eq. (7), in that the incident potential is continuous across that surface. Indeed, the potential jump on the near wake is only due to the scattered potential. Then, letting $\mathcal{S}_I$ approach $\mathcal{S}_W^F$, observing that the normal velocity component is continuous across a doublet layer, observing that the jump of the incident potential across it coincides with that of the scattered potential convected along the wake, that is,

$$\Delta\varphi_I(\boldsymbol{x}_W, t) = \Delta\varphi_S\left(\boldsymbol{x}_W^{\mathrm{TE}}, t - \tau\right) = \Delta\varphi(\boldsymbol{x}_W, t) \tag{8}$$

and comparing Eq. (7) with Eq. (5) yields

$$\int_{\mathcal{S}_B} \left(G \frac{\partial \varphi_I}{\partial n} - \varphi_I \frac{\partial G}{\partial n} \right) \mathrm{d}\mathcal{S}(\boldsymbol{y}) = 0 \tag{9}$$

The combination of Eq. (9) with Eq. (6) gives the following final integral equation for the scattered potential:

$$\varphi_S(\boldsymbol{x}, t) = \int_{\mathcal{S}_B} \left[G(\chi - \chi_I) - \varphi_S \frac{\partial G}{\partial n} \right] \mathrm{d}\mathcal{S}(\boldsymbol{y}) - \int_{\mathcal{S}_W^N} \Delta\varphi_S \frac{\partial G}{\partial n} \mathrm{d}\mathcal{S}(\boldsymbol{y}) \tag{10}$$

where the boundary conditions were expressed as $\partial\varphi_S/\partial n = \boldsymbol{v}_B \cdot \boldsymbol{n} - \boldsymbol{v}_I \cdot \boldsymbol{n} = \chi - \chi_I$, with the velocity induced by the far wake obtained from the gradient of Eq. (5) combined with Eq. (8), that is,

$$\boldsymbol{v}_I(\boldsymbol{x}, t) = -\nabla_{\boldsymbol{x}} \int_{\mathcal{S}_W^F} \Delta\varphi_S\left(\boldsymbol{y}_W^{\mathrm{TE}}, t - \tau\right) \frac{\partial G}{\partial n} \mathrm{d}\mathcal{S}(\boldsymbol{y}) \tag{11}$$

(the $\nabla_{\boldsymbol{x}}$ denotes the operation of gradient with respect to the variable $\boldsymbol{x}$). The incident potential influences the current scattered potential only by the induced-velocity term χ_I and, in turn, the scattered potential influences the incident potential by its trailing-edge discontinuity, which is convected along the wake and yields the intensity of the doublet distribution on the far wake. It is possible to show that the potential formulation outlined earlier is valid also for $\boldsymbol{x} \in \mathcal{S}_B$. In that case, Eq. (10) becomes an integral equation [9] that, solved by the boundary element approach described in the previous section, yields the scattered potential over the body.

The contribution of the far wake is evaluated by discretizing Eq. (11) through the N^F panels $\mathcal{S}_{W_n}^F$. This yields the following expression for the incident velocity field:

$$\boldsymbol{v}_I(\boldsymbol{x}, t) \approx -\sum_{n=1}^{N^F} \Delta\varphi_S\left(\boldsymbol{y}_{W_n}^{\mathrm{TE}}, t - \tau_n\right) \nabla_{\boldsymbol{x}} \int_{\mathcal{S}_{W_n}^F} \frac{\partial G}{\partial n} \mathrm{d}\mathcal{S}(\boldsymbol{y})$$

which, recalling the vortex-doublet equivalence [13–15], becomes

$$\boldsymbol{v}_I(\boldsymbol{x}, t) \approx \sum_{n=1}^{N^F} \Delta\varphi_S\left(\boldsymbol{y}_{W_n}^{TE}, t - \tau_n\right) \int_{\mathcal{C}_n} \nabla_{\boldsymbol{x}} G \times \mathrm{d}\boldsymbol{y} \tag{12}$$

where $\mathcal{C}_n = \partial\mathcal{S}_{W_n}^F$ is the shape of the vortex that replaces the effect of the doublets over the panel $\mathcal{S}_{W_n}^F$, and $\boldsymbol{y}_{W_n}^{\mathrm{TE}}$ denotes the trailing-edge position at which the wake material point currently in $\boldsymbol{y}_{W_n}$ emanated at time $t - \tau_n$. The superposition of the N^F closed vortices of shape $\mathcal{C}_n$ yields the vortex lattice through which the far wake is modeled (see Fig. 1). Equation (12) represents the velocity field given by the Biot–Savart law applied to the vortices having the shape of the panel contours and intensity $\Delta\varphi_S(\boldsymbol{y}_{W_n}^{\mathrm{TE}}, t - \tau_n)$. This field is equivalent and replaces the one that would be given by the gradient of the doublet distributions in the discretized form of Eq. (11). Equation (12) is applied both to evaluate the term χ_I appearing in Eq. (10) and to determine the contribution of the incident velocity field to the wake distortion during the free-wake analysis. In this formulation, numerical instability would occur when wake vortices come too close to each other or impinge the body (BVI) because of the singularities that would arise. A stable and regular solution is obtained by introducing in Eq. (12) a finite core vortex model that assumes a distribution of finite induced velocity within the core. In this work, the linear Rankine-vortex velocity distribution [16] is used within the core, although more complex core-velocity models are available in the literature (see, for instance, [17,18], in which velocity profiles having continuous derivatives across the core boundary were presented). This choice is motivated by the fact that for the configurations examined here, numerical investigations have shown that the final result is practically independent of the particular form of the core finite velocity (different velocity models with different core sizes may produce the same overall effect). The use of finite core vortices to describe the wake influence is a way to include also diffusivity and vortex-stretching effects that would be otherwise neglected in a potential-flow formulation (see [8,16,19] for details on this issue). Indeed, these effects do not play a crucial role in the prediction of pressure fields on lifting aeronautical configurations without massive separations, unless close or impinging interactions between bodies and wakes occur (as in BVI). In that case, the more realistic the modeling for the space wake vorticity distribution, the more accurate the simulation of the flowfield generated by the close wake-body interaction.

Once the potential field is known, the Bernoulli theorem yields the pressure distribution that, in turn, may be used both as part of an aeroelastic prediction tool to determine, for instance, the vibratory loads transmitted to the hub and as input to an aeroacoustic solver to predict the BVI-induced noise. Note that in this formulation, the explicit evaluation of the incident potential is required only in the Bernoulli theorem that, in a body-fixed frame of reference, reads

$$\dot{\varphi}_S + \dot{\varphi}_I - \boldsymbol{v}_B \cdot (\nabla\varphi_S + \boldsymbol{v}_I) + \frac{||\nabla\varphi_S + \boldsymbol{v}_I||^2}{2} + \frac{p}{\rho} = \frac{p_\infty}{\rho}$$

Here, the incident potential φ_I is obtained from integration of the incident velocity field given by Eq. (12), with inclusion of the vortex-core model.

This aerodynamic formulation could be extended to compressible flows by applying the theoretical development described here to the formulation presented in [9,10]. In that case, the solution algorithm would become much more complex and the computation much more time-consuming. Thus, the application of the compressible-flow formulation is convenient only if the inclusion of the compressibility effects is strictly necessary. In the following, the incompressible-flow formulation presented earlier is applied to rotors operating at subsonic Mach numbers in descent flight, for which the flowfield is dominated by BVI effects, rather than by flow compressibility.

IV. Numerical Results

To validate the present formulation, it is first compared with the standard panel method for the aerodynamic analysis of a helicopter rotor in a flight condition without BVI (i.e., a condition in which the standard formulation is applicable). To this aim, the scaled model of the Bo105 main rotor, examined within the European project HELINOISE, was considered [20]. This is a four-bladed model rotor with radius $R = 2.0$ m, constant chord $c = 0.121$ m, linear twist angle of -8 deg, coning angle of 2.5 deg, and modified NACA 23012 section profiles. The configuration examined is the climb forward flight, for which the effective tip-path plane is $\alpha_{\text{TPP}} = -14.63$ deg, the rotational speed is $\Omega = 108.9$ rad/s, and the advance ratio is $\mu = 0.148$. Figure 2 shows the comparison between the potential time history obtained by using the new aerodynamic formulation and that given by the standard one, under the assumption of incompressible flow. It concerns the point on the profile upper side located at the blade radial section $r = 0.75R$ and chordwise position $x = 0.04c$. The two results are virtually identical (the corresponding curves are nearly undistinguishable) and because the same agreement was observed over the whole blade surface, the formulation introduced in this work may be considered validated. Note that the scattered and the incident potentials defined here are of the same order of magnitude; hence, they are likewise significant in the evaluation of the total potential function.

The present formulation is next applied to helicopter rotors in BVI conditions. The rotors considered are the four-bladed EC/ONERA 7A and 7AD main rotors, which were examined at the DNW wind tunnel within the European project HELISHAPE [21]. These two rotors, both having an aspect ratio equal to 15, only differ by the shape of their tips. Specifically, rotor 7A has a rectangular tip, whereas rotor 7AD has a parabolic tip with taper, anhedral, and sweep angles. Both rotors are examined in 6-deg-descent, forward-flight condition, with rotational speed $\Omega = 101$ rad/s, advance ratio $\mu = 0.166$, and rotational tip Mach number $M_\Omega = 0.615$. The configurations analyzed are those related to the HELISHAPE Datapoint 70 for rotor 7A, and to the HELISHAPE Datapoint 108 for rotor 7AD. Because the purpose of the following numerical investigation is limited to the validation of the new aerodynamic formulation, the deformation of the blades was assumed to be linearly varying along the radial direction, with the tip-flap, lead-lag, and torsion deflections coinciding with those measured in the wind-tunnel tests. Furthermore, in the numerical analysis, the azimuthal step $\Delta\psi = 1.33$ deg was used and two wake spirals were included. In BVI conditions, the aerodynamic field is strongly dependent on the shape of the wake and on its distance from the rotor blades, and thus an accurate prediction of the distorted wake is essential. Figures 3 and 4 depict the rear and side views, respectively, of the distorted wake geometry given by the present free-wake analysis for rotor 7A. These figures clearly show that during the descent flight, the wake remains close to the rotor disk, thus inducing severe blade/wake impingement. In addition, for the sake of clarity, Fig. 5 depicts the wake of only one blade and shows the impact between one rotor blade and the wake generated by the preceding blade. A close view of the blade-wake impact is illustrated in Fig. 6, in which it is possible to observe that the computed wake-vortex filaments are not subject to strong distortion during the collision. Figures 5 and 6 concern the

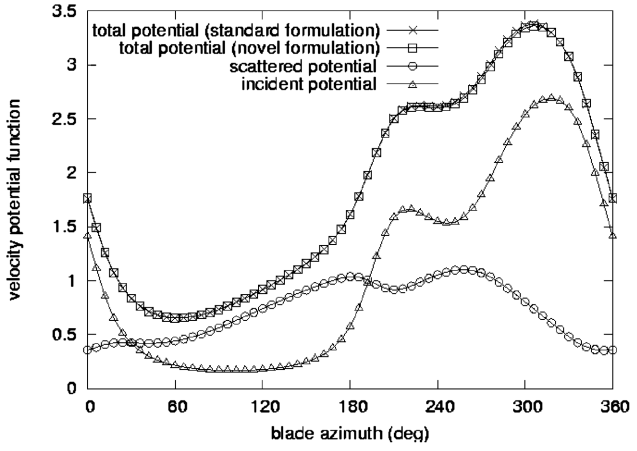

Fig. 2 Time history of the potential function at an upper-side blade point.

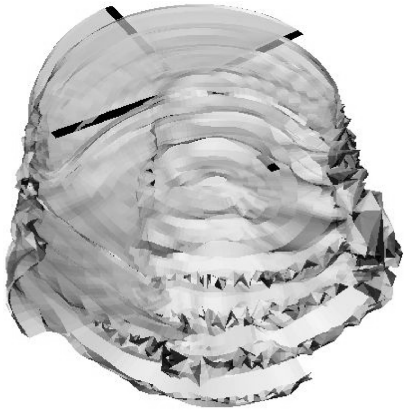

Fig. 3 Rotor 7A, rear view of computed wake geometry.

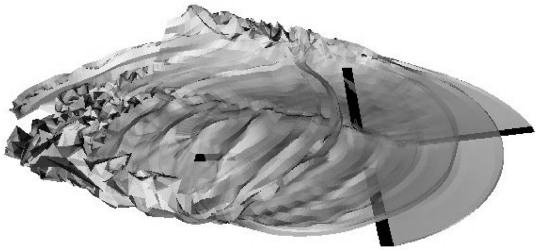

Fig. 4 Rotor 7A, side view of computed wake geometry.

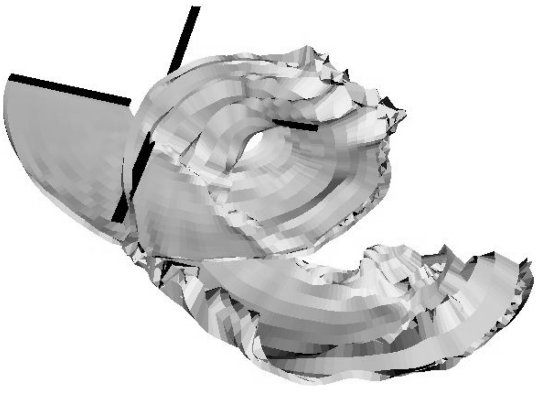

Fig. 5 Rotor 7A, blade/wake impingement.

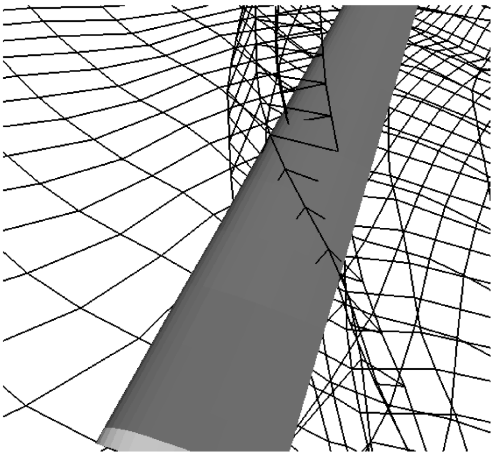

Fig. 6 Rotor 7A, blade/wake impingement (zoom).

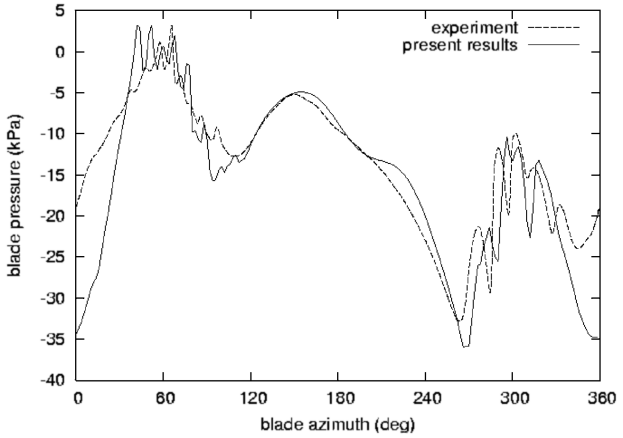

Fig. 7 Rotor 7A, time history of blade pressure at $r = 0.92R$ and $x = 0.02c$ (upper side).

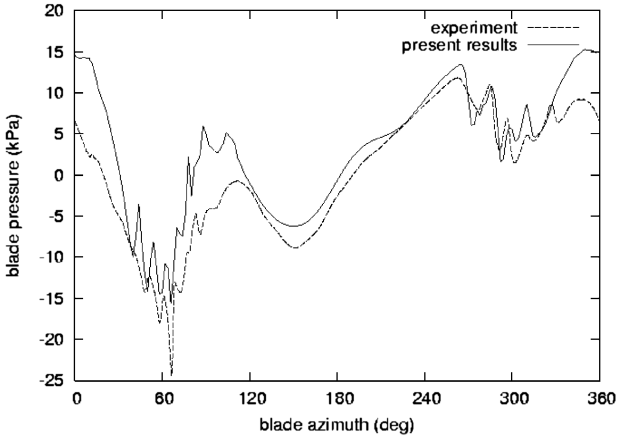

Fig. 8 Rotor 7A, time history of blade pressure at $r = 0.92R$ and $x = 0.02c$ (lower side).

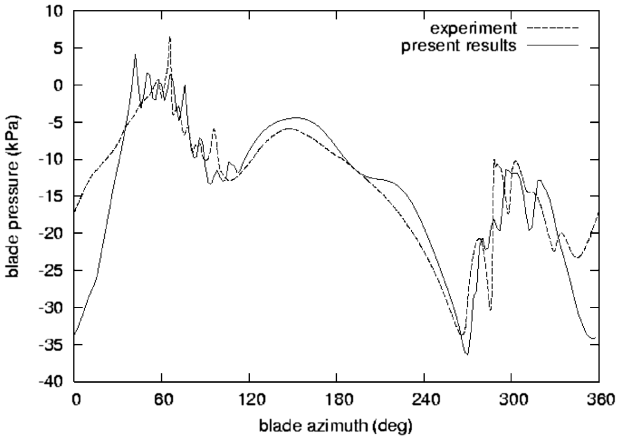

Fig. 9 Rotor 7AD, time history of blade pressure at $r = 0.92R$ and $x = 0.02c$ (upper side).

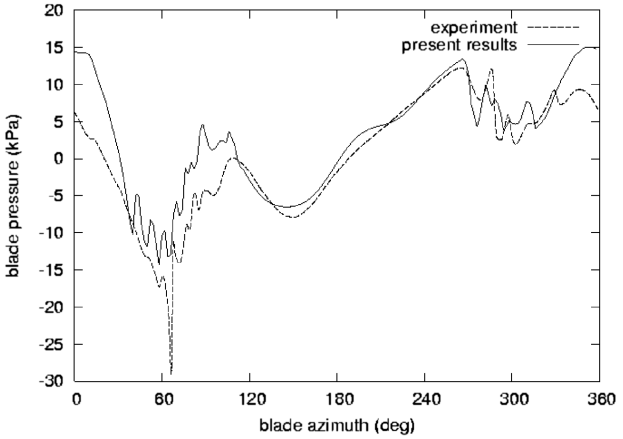

Fig. 10 Rotor 7AD, time history of blade pressure at $r = 0.92R$ and $x = 0.02c$ (lower side).

azimuth position $\psi = 65$ deg and indicate that the strongest BVI occurs at positions around $\psi = 60$ deg in the advancing side, although close blade/wake interaction also occurs around $\psi = 310$ deg in the retreating side. For this flight condition, the experimental measurements have detected strong BVI occurrence at azimuth positions around $\psi = 55$ deg [21]. Results concerning the computed blade pressure are then presented. Figures 7–10 depict, for rotors 7A and 7AD, the pressure time history on the profile upper and lower sides at $r = 0.92R$ and $x = 0.02c$. In these figures, the agreement between the numerical results and the experimental data is quite good, both in terms of detection of the regions in which BVI occurs and in terms of the order of magnitude of the pressure oscillations induced by BVI. Finally, some aeroacoustic results are presented. They are based on the blade pressure predicted by the aerodynamic solver and are obtained through the application of the Farassat [22] formulation 1A for the integration of the Ffowcs Williams and Hawkings equation [23]. This aeroacoustic formulation uses the free-space Green function and is valid for noise that propagates in a homogeneous medium without obstacles. Thus, for the prediction of noise produced by helicopters through inhomogeneous media in the presence of scattering surfaces (as is required for the simulation of flights close to terrain and buildings), the present aeroacoustic approach could be applied to get the near-field solution on a surface around the aircraft, which would in turn become the starting point of a far-field propagation methodology [24]. A procedure of this type is often used in noise-optimization processes. Figures 11–16 present the comparison between the measured acoustic pressure and the acoustic time signature given by the numerical predictions. Figures 11–13 concern rotor 7A, Figs. 14–16 concern rotor 7AD, and these two groups of figures are related to the same observer positions. These observers are located 2.286 m below the rotor disk. In the experimental tests, the first one (observer A) corresponds to the upstream microphone 3 that is 2 m distant from the rotor hub (advancing rotor side), the second one (observer B) corresponds to the upstream microphone 3 located 3 m far from the rotor hub (advancing rotor side), and the third one (observer C) corresponds to the upstream microphone 9 that is 3.5 m far from the rotor hub (retreating rotor side). The acoustic correlations show that for both rotors, although the numerical results present a bit more oscillating behavior with respect to the experimental data, the impulsiveness of the signal and the intensity of

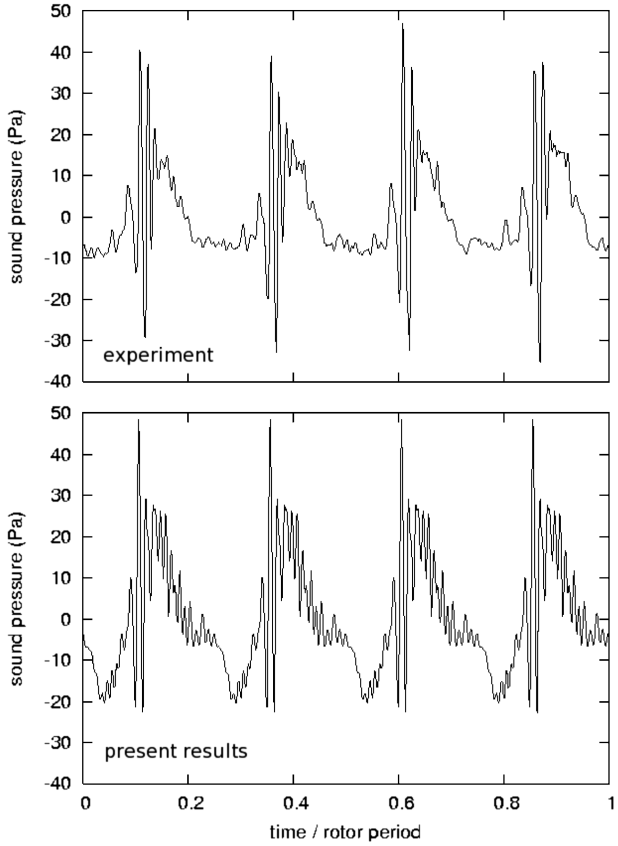

Fig. 11 Rotor 7A, experimental and numerical acoustic signature at observer A.

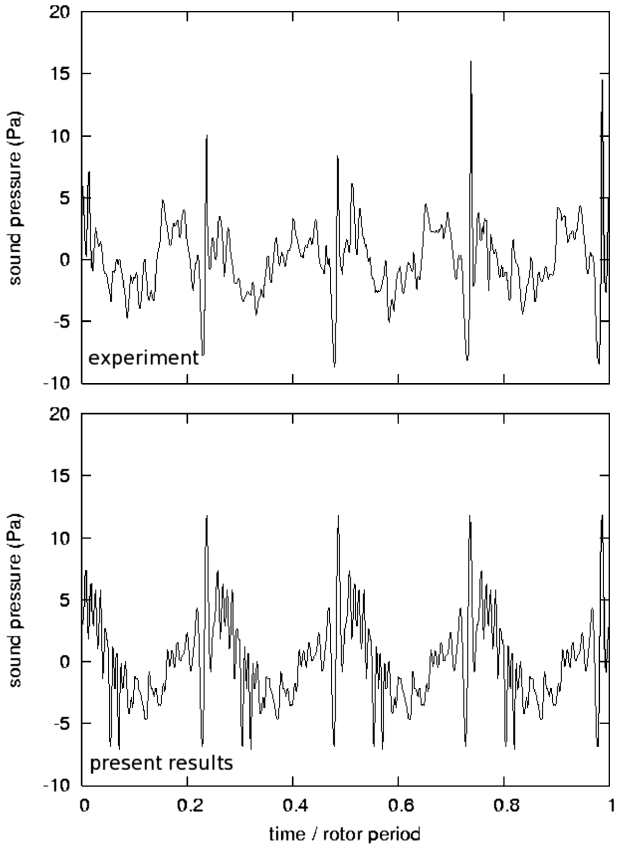

Fig. 13 Rotor 7A, experimental and numerical acoustic signature at observer C.

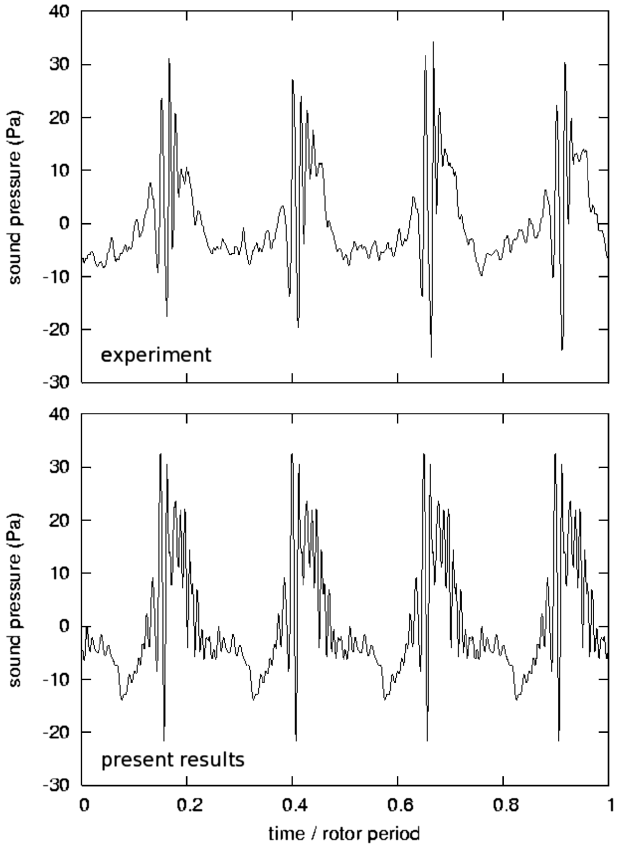

Fig. 12 Rotor 7A, experimental and numerical acoustic signature at observer B.

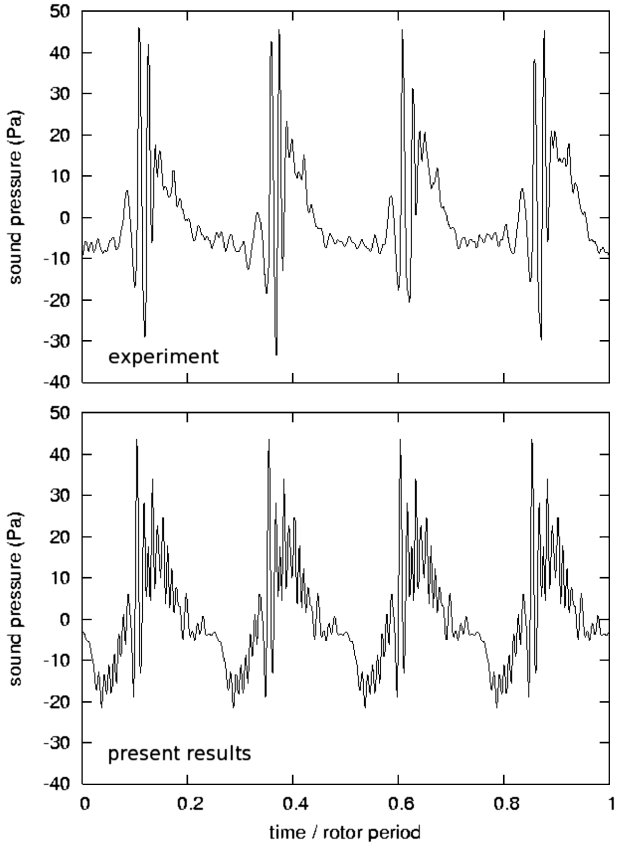

Fig. 14 Rotor 7AD, experimental and numerical acoustic signature at observer A.

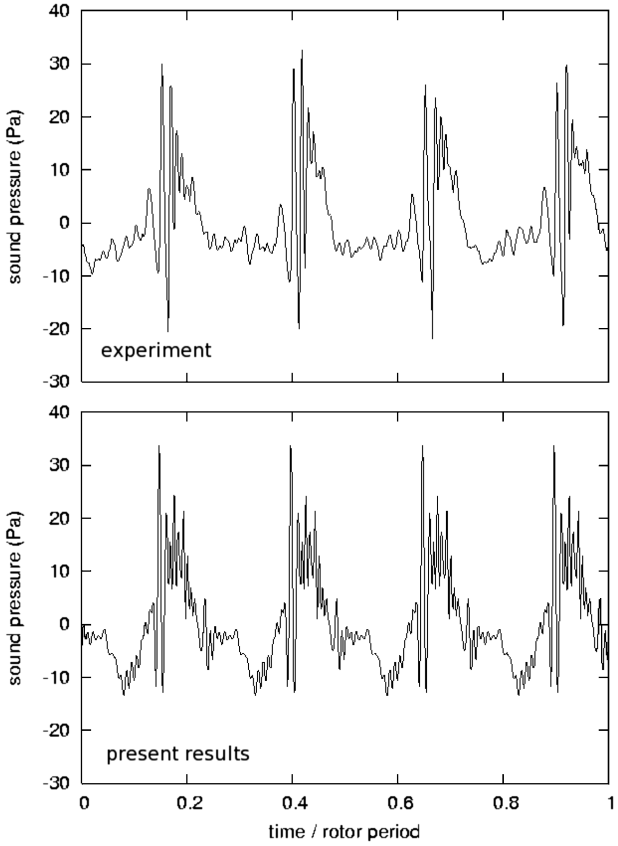

Fig. 15 Rotor 7AD, experimental and numerical acoustic signature at observer B.

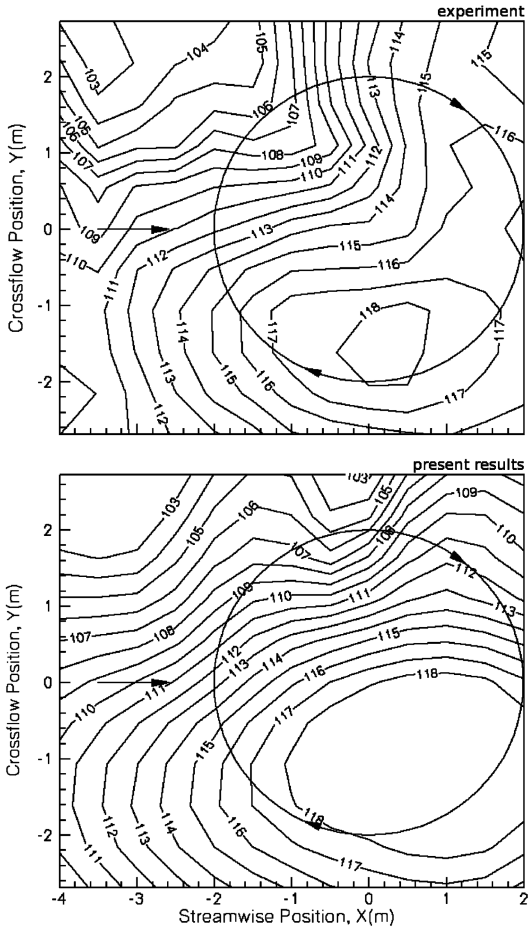

Fig. 17 Rotor 7A, noise contour levels (dB).

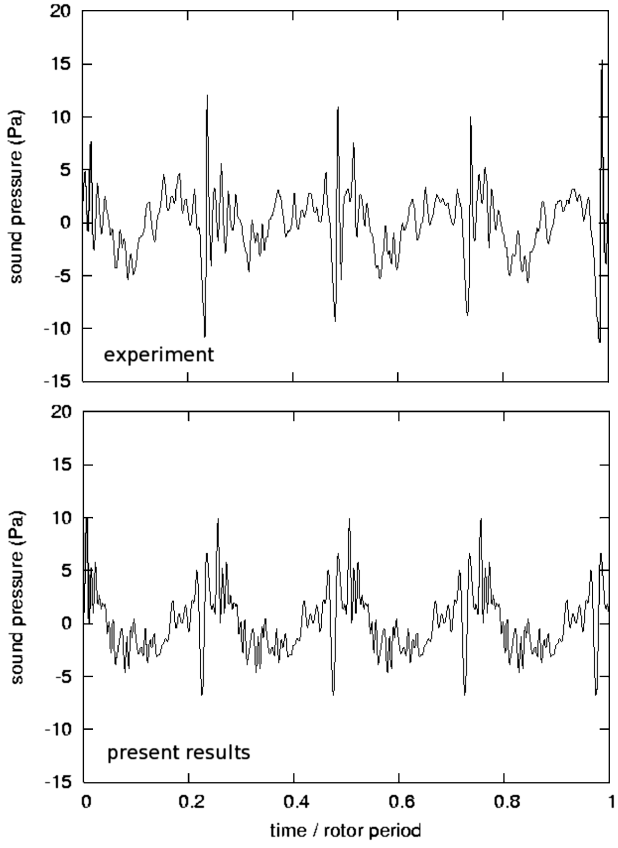

Fig. 16 Rotor 7AD, experimental and numerical acoustic signature at observer C.

the peaks due to BVI are in good agreement with the wind-tunnel measurements. The overall quality of the numerical predictions can be assessed from Figs. 17 and 18, which concern the noise contour levels (expressed in dB) related to the arrays of microphones positioned on the horizontal plane located 2.286 m below the rotor disk. Results from experimental data and numerical analysis for rotor 7A are given in Fig. 17, and Fig. 18 is related to rotor 7AD. For both rotors, the contour levels show a region of a high level of noise radiated from BVI on the advancing rotor side, and a region of a low level of radiated noise in the upstream retreating rotor side. These figures demonstrate that the numerical results correlate quite well with those from the measurements, in terms of both noise directivity and noise intensity.

V. Conclusions

A direct panel method that is suited for the aerodynamic analysis of helicopter rotors in BVI conditions was introduced. It is applicable to arbitrarily shaped, thick blade rotors in arbitrary flight motion. This formulation yields a unified approach for wake-deformation analysis and blade-pressure prediction. For a helicopter rotor configuration in which no BVI occurs, the formulation presented gives the same aerodynamic solution obtained by the standard direct panel method. Considering helicopter rotors in BVI configurations, stable and regular solutions were obtained by expressing the influence of the wake portion experiencing BVI on the potential field in terms of a finite thickness vortex lattice. The numerical results demonstrated the capability of the present approach to identify realistic distorted wake shapes that correlate well with the wakes visualized in the wind-tunnel tests. BVI occurrence is properly predicted, and the agreement between numerical results and wind-tunnel measurements is good, both in terms of blade-pressure correlation and in terms of acoustic signature correlation. This

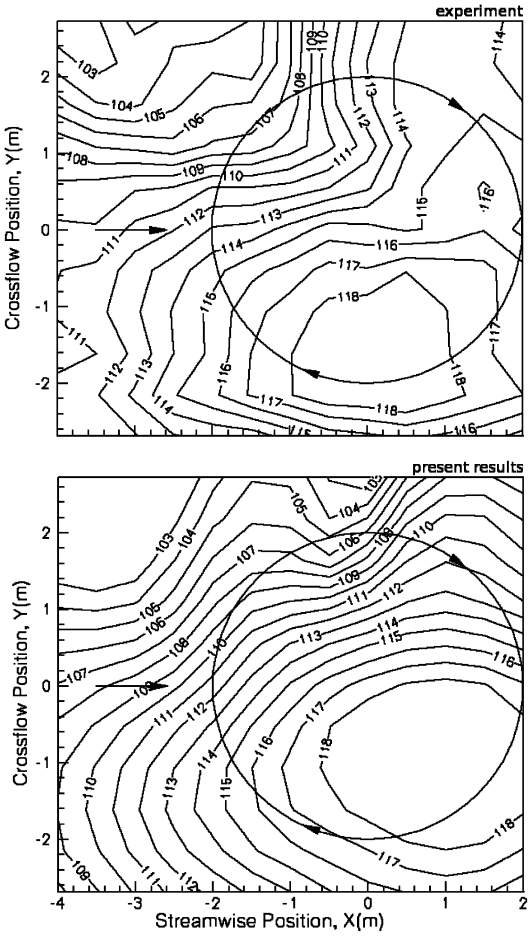

Fig. 18 Rotor 7AD, noise contour levels (dB).

formulation can be extended to compressible flows and can be used for a unified aerodynamic/aeroacoustic analysis.

Acknowledgments

This work was partially supported by the European Union Integrated Project FRIENDCOPTER (contract no. AIP3-CT-2003-502773). The authors wish to thank S. Ianniello for his help in obtaining the aeroacoustic results presented.

References

[1] Tung, C., Yu, Y. H., and Low, S. L., "Aerodynamic Aspects of Blade–Vortex Interaction (BVI)," 27th AIAA Fluid Dynamics Conference, New Orleans, LA, AIAA Paper 96-2010, 1996.

[2] Lim, J. W., Yu, Y. H., and Johnson, W., "Calculation of Rotor Blade–Vortex Interaction Airloads Using a Multiple-Trailer Free-Wake Model," *Journal of Aircraft*, Vol. 40, No. 6, 2003, pp. 1123–1130.

[3] Munsky, B., and Gandhi, F., "Analysis of Helicopter Blade–Vortex Interaction Noise with Flight Path or Attitude Modification," *Journal of the American Helicopter Society*, Vol. 50, No. 2, 2005, pp. 123–137.

[4] Patt, D., Liu, L., and Friedmann, P. P., "Rotorcraft Vibration Reduction and Noise Predictions Using a Unified Aeroelastic Response Simulation," *Journal of the American Helicopter Society*, Vol. 50, No. 1, 2005, pp. 95–106.

[5] Beaumier, P., and Delrieux, Y., "Description and Validation of the ONERA Computational Methods for the Prediction of Blade–Vortex Interaction Noise," *Aerospace Science and Technology*, Vol. 9, No. 1, 2005, pp. 31–43.

[6] Ahmed, S. R., and Vidjaja, V. T., "Unsteady Panel Method Calculation of Pressure Distribution on BO 105 Model Rotor Blades," *Journal of the American Helicopter Society*, Vol. 43, No. 1, 1998, pp. 47–56.

[7] Morino, L., "A General Theory of Unsteady Compressible Potential Aerodynamics," NASA CR-2464, 1974.

[8] Morino, L., and Bharadvaj, B. K., "A Unified Approach for the Potential and Viscous Free-Wake Analysis of Helicopter Rotors," *Vertica*, Vol. 12, Nos. 1–2, 1988, pp. 147–154.

[9] Morino, L., and Gennaretti, M., "Boundary Integral Equation Methods for Aerodynamics", *Computational Nonlinear Mechanics in Aerospace Engineering*, edited by S. N. Atluri, Vol. 146, Progress in Aeronautics and Astronautics, AIAA, Washington, D.C., 1992, pp. 279–320.

[10] Morino, L., Bernardini, G., and Gennaretti, M., "A Boundary Element Method for the Aerodynamics and Aeroacoustics of Bodies in Arbitrary Motions," *International Journal of Aeroacoustics*, Vol. 2, No. 2, 2003, pp. 129–156.

[11] Gennaretti, M., Luceri, L., and Morino, L., "A Unified Boundary Integral Methodology for Aerodynamics and Aeroacoustics of Rotors," *Journal of Sound and Vibration*, Vol. 200, No. 4, 1997, pp. 467–489.

[12] Morino, L., and Bernardini, G., "Singularities in Discretized BIE's for Laplace's Equation: Trailing-Edge Conditions in Aerodynamics," *Mathematical Aspects of Boundary Element Methods*, edited by M. Bonnet, A. M. Sändig, and W. L. Wendland, Chapman and Hall/CRC, London, 2000, pp. 240–251.

[13] Campbell, R. G., *Foundations of Fluid Flow Theory*, Addison–Wesley, Reading, MA, 1973.

[14] Morino, L., "Boundary Integral Equations in Aerodynamics," *Applied Mechanics Reviews*, Vol. 46, No. 8, 1993, pp. 445–466.

[15] Gennaretti, M., Giordani, A., and Morino, L., "A Third-Order Boundary Element Method for Exterior Acoustics with Applications to Scattering by Rigid and Elastic Shells," *Journal of Sound and Vibration*, Vol. 222, No. 5, 1999, pp. 699–722.

[16] Leishman, J. G., *Principles of Helicopter Aerodynamics*, Cambridge Univ. Press, Oxford, England, U.K., 2000.

[17] Vatistas, G. H., Kozel, V., and Mih, W. C., "A Simpler Model for Concentrated Vortices," *Experiments in Fluids*, Vol. 24, No. 11, 1991, pp. 73–76.

[18] Krasny, R., and Nitsche, M., "The Onset of Chaos in Vortex Sheet Flow," *Journal of Fluid Mechanics*, Vol. 454, Mar. 2002, pp. 47–69.

[19] Ananthan, S., and Leishman, J. G., "Role of Vortex Filament Stretching in the Modeling of Rotor Wakes," *Journal of the American Helicopter Society*, Vol. 49, No. 1, 2004, pp. 176–191.

[20] Splettstoesser, W. R., Junker, B., Schultz, K. J., Wagner, W., Weitemeyer, W., Protopsaltis, A., and Fertis, D., "The HELINOISE Aeroacoustic Rotor Test in the DNW-Test Documentation and Representative Results," *DLR-Mitteilung*, Vol. 93-09, 1993.

[21] Schultz, K. J., Splettstoesser, W., Junker, B., Wagner, W., Schoell, E., Mercker, E., Pengel, K., Arnaud, G., and Fertis, D., "A Parametric Wind Tunnel Test on Rotorcraft Aerodynamics and Aeroacoustics (Helishape)—Test Procedures and Representative Results," *The Aeronautical Journal*, Vol. 101, No. 1004, 1997, pp. 143–154.

[22] Farassat, F., "Linear Acoustic Formulas for Calculation of Rotating Blade Noise," *AIAA Journal*, Vol. 19, No. 9, 1981, pp. 1122–1130.

[23] Ffowcs Williams, J. E., and Hawkings, D. L., "Sound Generation by Turbulence and Surfaces in Arbitrary Motion," *Philosophical Transactions of the Royal Society of London, Series A: Mathematical and Physical Sciences*, Vol. A264, No. 1151, 1969, pp. 321–542.

[24] Conner, D. A., and Page, J. A., "A Tool for Low Noise Procedures Design and Community Noise Impact Assessment: The Rotorcraft Noise Model (RNM)," *Proceedings of the AHS International Meeting on Advanced Rotorcraft Technology and Life Saving Activities*, Heli Japan, Tochigi-kan, Japan, 2002, pp. T213-6-1–T213-6-11.

K. Ghia
Associate Editor